Locally induced quantum interference in scanning gate experiments

2014 New J. Phys. 16 053031

(http://iopscience.iop.org/1367-2630/16/5/053031)

New Journal of Physics
The open access journal at the forefront of physics
Deutsche Physikalische Gesellschaft DPG | IOP Institute of Physics

Locally induced quantum interference in scanning gate experiments

A A Kozikov, R Steinacher, C Rössler, T Ihn, K Ensslin, C Reichl and W Wegscheider

Solid State Physics Laboratory, ETH Zürich, CH-8093 Zürich, Switzerland
E-mail: akozikov@phys.ethz.ch

Received 10 October 2014, revised 5 April 2014
Accepted for publication 9 April 2014
Published 16 May 2014

New Journal of Physics **16** (2014) 053031

doi:10.1088/1367-2630/16/5/053031

Abstract

We present conductance measurements of a ballistic circular cavity influenced by a scanning gate. In contrast to previous studies, we demonstrate the use of scanning gate microscopy as a tool for tailoring the potential landscape of nanostructures with a high degree of control. When the tip depletes the electron gas below, we observe very pronounced and regular fringes covering the entire cavity. The fringes correspond to transmitted modes in constrictions formed between the tip-induced potential and the boundaries of the cavity. Moving the tip and counting the fringes gives us exquisite control over the transmission of these constrictions. We use this control to form a quantum ring with a specific number of modes in each arm showing the Aharonov–Bohm effect in low-field magnetoconductance measurements.

Keywords: quantum interference, scanning probe microscopy, high-mobility GaAs/AlGaAs

1. Introduction

Semiconductor nanostructures are usually defined electrostatically using top–down or bottom–up approaches. For example, one can use suitably biased lateral gates or self-assembled systems based on sophisticated growth schemes to prepare semiconductor quantum structures. In all these cases, the main features of the potential landscape are defined for each

sample and are only weakly tunable. Using the conductive tip of a scanning force microscope as a movable top gate allows for more advanced control over the potential. In addition to the tip-sample bias voltage, the tip-surface distance and the in-plane tip position can be changed. The variable strength and gradient of the tip-induced potential provides one with the possibility of tailoring the potential landscape of nanostructures. In the past this scanning gate microscopy (SGM) technique was used to study the conductance of predefined nanostructures. For example, Topinka *et al*, Paradiso *et al* and Kozikov *et al* imaged electron backscattering through a quantum point contact (QPC) [1–4]. These experiments demonstrated that SGM allows one to observe features smaller than the Fermi wavelength. In addition, Pioda *et al* and Fallahi *et al* looked into single electron transport in quantum dots [5, 6] and Woodside *et al* in carbon nanotubes [7]. Hackens *et al* probed electron transport through a quantum ring [8, 9].

In this paper, we demonstrate how to extend this technique to alter the potential landscape in a ballistic cavity using a scanning gate. In the previous paper [10] we showed how to form QPCs with the SGM tip at the openings of the cavity. At the same time, everywhere else inside the cavity we observed irregular conductance fluctuations governed by chaotic electron dynamics or disorder. This irregular behavior is similar to that observed in previous SGM studies of ballistic cavities [11, 12]. The formation of the QPCs with the tip demonstrates the possibility of using SGM as a tool to alter the potential landscape in order to form more complex nanostructures. We observe regular modulations and fringe patterns in the spatially resolved conductance covering the entire ballistic cavity in contrast to the previous studies [10–12]. The control achieved over the potential landscape is used to form a quantum ring showing Aharonov–Bohm oscillations. This requires to have a spatially and temporally very stable setup. The observation of the Aharonov–Bohm oscillations in our samples testifies to the quality of our experimental setup as well as to the potential to investigate quantum effects in more detail in complex nanostructures whose potential can be tailored with the scanning gate.

2. Experimental methods

The microstructure is fabricated on a high-mobility GaAs/AlGaAs heterostructure. The electron gas buried 120 nm beneath the surface has a mobility of 3.8×10^6 cm^2 Vs^{-1} at 300 mK at a carrier density of 1.5×10^{11} cm^{-2}. This gives an elastic mean free path $l_e = 50\ \mu$m and a Fermi wavelength of electrons $\lambda_F = 65$ nm.

The device under study consists of three circular stadii connected in series with different lithographic diameters 1.0, 1.2 and 1.5 μm. In this paper we focus on the largest cavity with the diameter $D = 1.5\ \mu$m, which is shown in figure 1 (a). The structure is defined by applying a negative voltage to the corresponding metallic gate electrodes t_1, t_2, t_3, $b_1$and $b_2$fabricated by e-beam lithography, each 30 nm high. The electron gas beneath them becomes depleted at -0.4 V. Since $D \ll l_e$, transport through the cavity is ballistic. At the same time $D \gg \lambda_F$.

The measurements are performed in a ^{3}He system with a base temperature of 300 mK using a home-built scanning force microscope [13]. The two-terminal linear conductance G through the device is measured by applying a 26 Hz ac rms voltage of 100 μV between the source and drain contacts. Scanning gate measurements are performed by placing the metallic biased tip of the scanning force microscope 60 nm above the sample surface. The tip scans the surface at a constant height and G is recorded simultaneously leading to 2D maps $G\left(x, y\right)$ as a

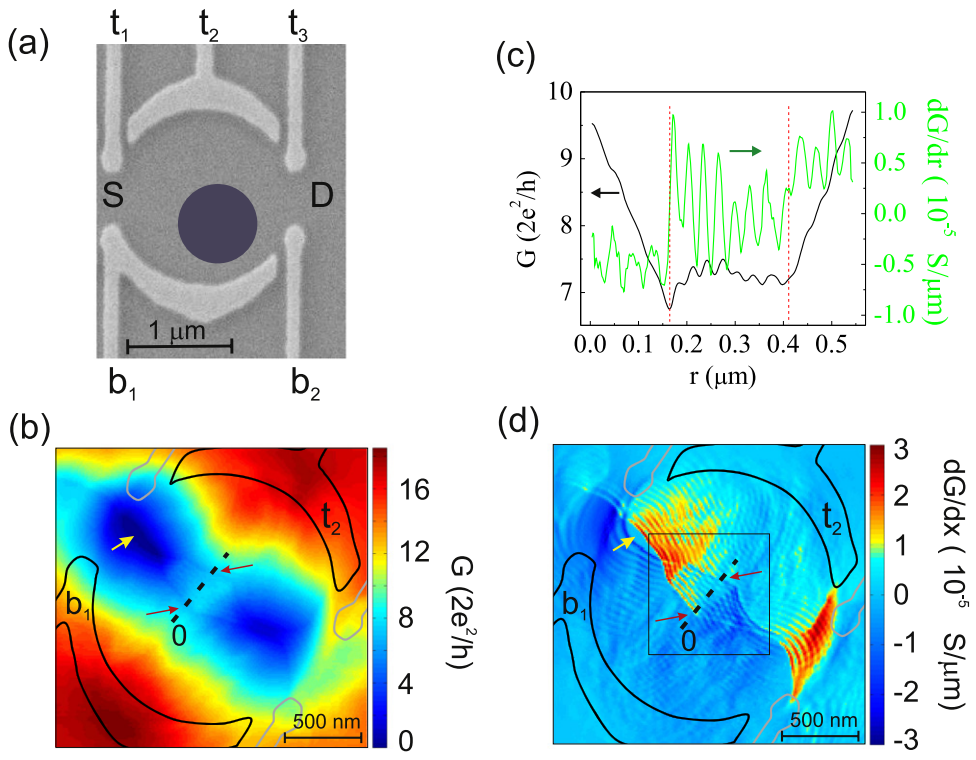

Figure 1. (a) SEM image of the device. The dark grey area corresponds to the GaAs surface, bright grey regions labeled t_1, t_2 and t_3, b_1 and b_2 are metallic top gates. The ac current flows between the source 'S' and drain 'D' contacts. The size of the tip-depleted disc is schematically represented by the dark blue circle. (b) Conductance, G, through the cavity in units of $2e^2/h$ as a function of tip position, (x,y). The biased t_2 and b_1 and grounded t_1, t_3 and b_2 top gates are outlined by black and grey solid lines, respectively. (c) Conductance and its numerical derivative along the black dashed line shown in (b). Vertical red dashed lines in (c) together with red arrows in (b) mark the borders of the checker-board pattern. The coordinate $r = 0$ μm is labeled at the left end of the black dashed line. (d) Numerical derivative of the conductance in (b), $\mathrm{d}G\left(x, y\right)/\mathrm{d}x$, as a function of tip position. The black dashed line is at the same position as that in (b). The black square is the region where high-resolution measurements are taken. Yellow arrows in (b) and (d) mark the lens-shaped region of zero conductance arising when the tip is close to the left constriction. Voltages -0.5 and -4.0 V are applied to the top gates and the tip, respectively. The tip is placed 60 nm above the GaAs surface. Biased top gates are labeled in (b) and (d).

function of lateral tip position (x,y). A voltage of -4 V between the tip and the 2DEG is chosen to deplete the electron gas beneath the tip. The resulting diameter of the depletion region is about 0.7 μm [10].[1]

[1] The presence of the lens-shaped region of zero conductance in a region where the cavity connects to the leads indicates that the tip-depleted region is larger than this opening, which in our case is $W \approx 0.6$ μm wide (the width of the left opening in figure 1(d) at the studied gate voltage is approximately equal to its lithographic width). If this region were a line, then the diameter of the tip-depleted region was $D_{\mathrm{Tip}} = W = 0.6$ μm. In the experiment this region has the shape of a lens. With respect to the center of the constriction (center of the lens-shaped region) the tip can move up and down by half the width of the lens, $l/2 \approx 50$ nm, still blocking the current. Thus, the final $D_{\mathrm{Tip}} = W + l \approx \left(0.6 + 0.1\right)$ μm $= 0.7$ μm.

Figure 1(b) shows the conductance through the cavity in color when a voltage of -0.5 V is applied to the top gates t_2 and b_1 outlined with black solid lines. This voltage reduces the electronic size of the structure by about 100 nm compared to the geometric size. When the tip is inside the structure, G decreases from the tip-unpertubed value $G \approx 17.2 \times 2e^2/h$ to zero (lens-shaped regions of dark blue color marked by the yellow arrow). Such a drop of the conductance is due to backscattering of electrons at the tip-depleted region. As the tip comes close enough to one of the constrictions, its depletion disc blocks the current entirely. The conductance is not reduced to zero when the tip is close to the right constriction, because this constriction is larger than the left. When the tip is above the top gates or outside the structure, the conductance is enhanced to $G \approx 18.5 \times 2e^2/h$ (dark red area) compared to G without the tip. Such an enhancement has been observed by us in seven different stadii, four of which have different diameters. Qualitatively it is due to a tip-induced transition from Ohmic to adiabatic transport [10, 14]. The tip potential guides electrons adiabatically through the cavity enhancing the conductance compared to the situation in which the total resistance is roughly the sum of resistances of the entrance and exit of the cavity. Transport is in both cases dominated by the resistance of the narrowest constriction.

On closer inspection one can see faint fringes in the central region (along the dashed line between two red arrows) of the cavity. Figure 1(c) shows the corresponding conductance along the black dashed line in (b). Indeed, G oscillates in this region (enclosed between the two vertical red lines) and stays on average roughly at a constant value of $G \approx 7 \times 2e^2/h$. Such behavior can intuitively arise from the formation of two narrow channels between the tip-depleted region and t_2 and b_1 each having its own quantized conductance G_1 and G_2. Classically the total conductance would then be $G = G_1 + G_2$. Outside the central region one of these channels is depleted and G is determined by the remaining channel, i.e. either G_1 or G_2. As this channel becomes wider, G increases steeply as seen in the two regions outside the vertical dashed red lines. Small 'shoulders' in G seen in these two regions correspond to quantized conductance of the remaining channel. The 'shoulders' do not appear at integer multiples of $2e^2/h$, because of the tip position dependent series resistance, interference [10] and backscattering effects [4]. Such small modulation of G can be revealed by taking a numerical derivative $\mathrm{d}G\left(r\right)/\mathrm{d}r$ (green curve in figure 1(c)). Conductance oscillations are now clearly seen along the entire length of the chosen 1D cut.

To reveal such small changes in G in the entire area of figure 1(b), a numerical derivative $\mathrm{d}G\left(x, y\right)/\mathrm{d}x$ with respect to the scan direction is plotted in figure 1(d). Several fringe patterns covering the entire structure are now visible. Two of them are located at the left constriction around the lens-shaped region (marked by the yellow arrow) and at the right constriction. These fringes originate from conductance quantization in single QPCs formed between the tip-induced potential and the boundaries of the cavity [10]. For example, when the tip moves from the left lens-shaped region towards the top gate t_2, a constriction opens gradually between the tip and the lower top gate b_1. As its width increases, more modes are transmitted through it. Each added mode corresponds to one fringe period. The fringe spacing in the image is not constant because the constriction width depends on the subband spacing and because the carrier density inside these constrictions changes by the tip-induced potential.

Each fringe at the left lens-shaped region in figure 1(d) evolves continuously through the center of the cavity to a corresponding fringe at the right constriction. This gives rise to a

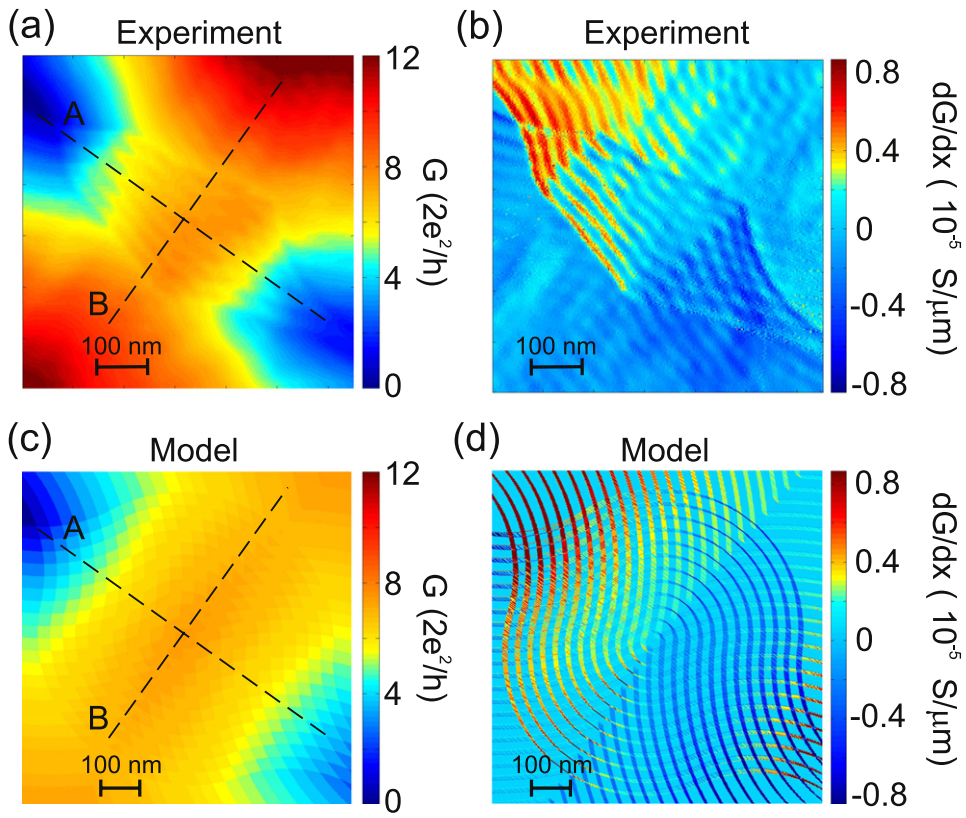

Figure 2. (a) Conductance, $G\left(x, y\right)$, through the cavity 1.5 μm in diameter in units of $2e^2/h$ as a function of tip position in the region indicated in figure 1(d) by a square. (b) Numerical derivative of the conductance in (a), $dG\left(x, y\right)/dx$. The top gates and the tip are biased to -0.5 and -4.0 V, respectively. (c) Modeled conductance and (d) its numerical derivative.

checkerboard pattern formed in the central region of the structure. The 1D cut discussed in (c) is taken across this pattern (its borders are marked by the same red arrows as in (b)).

To check the proposed origin of the checkerboard pattern in the center of the cavity, we take a separate high-resolution measurement of this region and compare the results with computer modeling. Figure 2 shows the mentioned checkerboard pattern both in the raw conductance (a) and in its numerical derivative (b). In order to model this situation, we consider four constrictions: two, a and b, at the entrance and exit of the cavity. The two others, c and d, form between the tip-depleted region and either gate t_2 or b_1 [10]. We treat them as four incoherently coupled conductors. The total conductance is then $G^{-1} = G_a^{-1} + \left(G_c + G_d\right)^{-1} + G_b^{-1}$. The conductance of each constriction is taken to be $G_i = \left(2e^2/h\right) \times N_i$ (i = a, b, c and d), where $N_i = 2W_i/\lambda_F$ is the number of transmitted modes in constriction i and W_i is the width of constriction i. As the tip moves, only N_c and N_d change in our model for simplicity. The numbers $N_a = 18$ ($W_a = 0.6$ μm) and $N_b = 25$ ($W_b = 0.8$ μm) are kept fixed. The resulting G and $dG\left(x, y\right)/dx$ are shown in figure 2(c) and (d), respectively, as a function of tip position.

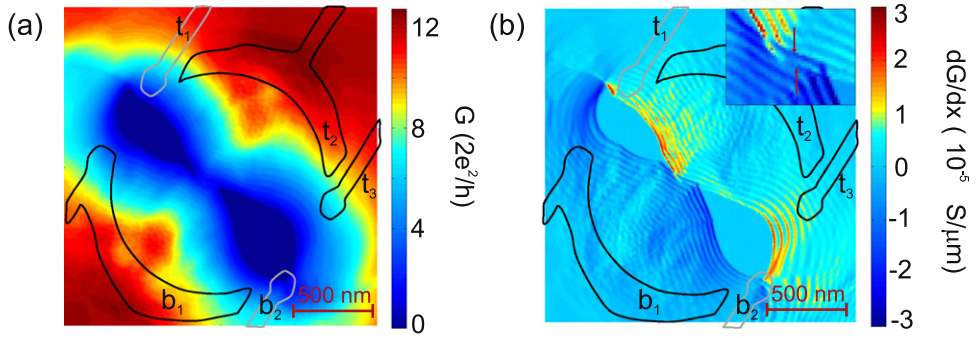

Figure 3. (a) Conductance, $G\left(x,\, y\right)$, through the largest cavity. The top gates are now biased (black solid lines) to form a more symmetric cavity. The grounded top gates are indicated by grey solid lines. (b) Numerical derivative of the conductance in (a), $\mathrm{d}G\left(x,\, y\right)/\mathrm{d}x$. The inset is the central region of the cavity enlarged for clarity. The red arrows indicate two fringes each corresponding to one transmitted mode in each arm of the ring. All top gates are labeled.

The model shows a reasonable qualitative and quantitative agreement with the experimental data along line A shown in figure 2(a) and (c). Along line B the agreement is only qualitative. This is because the model does not take into account the tip-induced transition from Ohmic to adiabatic transport. In addition, the tip-induced potential in the model is assumed to be a hard-wall and the four conductors are incoherently coupled. The latter is a rough approximation. When the tip is in the central part of the cavity, it forms an electronic ring together with the boundaries of the cavity (gates t_2 and b_1). Since each arm gives its own set of parallel fringes, a checkerboard pattern forms in the model in figure 2(d) similar to the experimental observation in figure 2(b). The shape of the fringes follows the inner edge of the respective top gate. The experiment shows rather sharp kinks in the fringe pattern, whereas the simulation does not. This could arise, because the tip-induced potential or the electrostatic edges of the cavity may not be perfectly round.

Counting the measured fringes enables us to determine and then set the exact number of transmitted modes in the constrictions formed between the tip-induced potential and the boundaries of the cavity. Having such an exquisite control allows us to tune the system to form an Aharonov–Bohm ring with a specific number of modes in each arm. As an example, in figure 3 voltages are applied to the gates b_1, t_2 and t_3 to have a symmetric cavity (note that the lens-shaped regions are almost the same size) with only two fringes in its middle (see inset of figure 3(b)). The number of fringes in the checkerboard pattern yields the number of transmitted modes in each arm of the ring. Placing the tip between these two fringes (inset in figure 3(b)) and in the middle between the lens-shaped regions forms the desired Aharonov–Bohm (AB) ring. We tune the entrance and exit of this ring to transmit only a few modes. For this purpose, after fixing the tip position as described, the two previously grounded gates t_1, b_2 are biased to the same voltage of -0.5 V. The conductance, $G\left(B,\, V_{\mathrm{g}}\right)$, is then measured as a function of the magnetic field and the voltage applied to all top gates of the structure.

The resulting $G\left(B,\, V_{\mathrm{g}}\right)$ taken at a source-drain bias of 10 μV are presented in figure 4 (a). They show a small (about 0.3%) modulation of G marked by black arrows. Subtracting a slowly

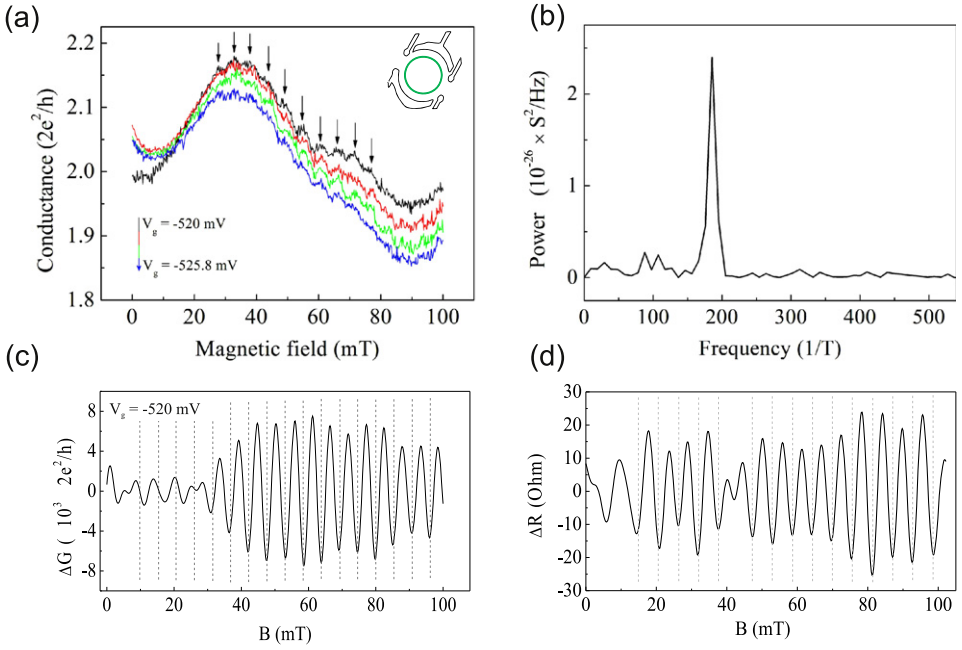

Figure 4. (a) Low-field magnetoconductance measured through a tip formed ring. Curves of different colors correspond to different gate voltages with a step of -1.93 mV. The inset shows a schematic of the tip-formed Aharonov–Bohm ring. (b) A Fourier spectrum of the black curve in (a) with the subtracted background. (c), (d) Filtered data from two- and four-terminal measurements, respectively. Equidistantly spaced vertical dashed lines are guides to the eye.

varying background due to classical effects and taking a Fourier spectrum reveals a single peak at a frequency of about 185 T^{-1} (figure 4(b)). This peak corresponds to an oscillation period of 5.4 mT, which agrees roughly with the h/e period of a ring with an estimated diameter of 1 μm. One conductance curve band-pass filtered around the peak in the Fourier spectrum is shown in figure 4(c).

The AB oscillations are found to be very sensitive to the tip position on the scale of half the Fermi wavelength. They exist only in a narrow range of gate voltages. Nevertheless, the oscillations were reproducibly found in different cooldowns and with different tips measured in two- and four-terminal configuration. As an example, we present in figure 4(d) the result of the filtered data similar to those shown in figure 4(c) but obtained using a four-terminal configuration by passing a current of 1 nA through the sample. The relative amplitudes of the AB oscillations in two- (about 0.3%) and four-terminal (about 0.5%) measurements are very similar.

3. Conclusion

We have presented results of transport measurements through a ballistic circular cavity, the potential of which was modified by a scanning gate. Conductance maps as a function of tip position revealed fringe patterns covering the entire structure. The fringes correspond to conductance quantization plateaus in constrictions formed between the tip-induced potential and the boundaries of the cavity. At the entrance and exit of the cavity the tip formed single

constrictions together with either gate of the cavity. This lead to single sets of fringes. In the center of the microstructure they crossed each other, forming a checkerboard pattern—corresponding to a situation when the tip created a quantum ring. Transport in this case occurred through both arms of the ring. Results of computer modeling agreed qualitatively with our experimental observations.

To transmit through the cavity, electron waves are split into two by the tip and interfere when recombined at the other side. By counting the fringes, a specific number of transmitted modes in the arms of the ring was set. As a result we observed conductance oscillations as a function of low magnetic field due to the Aharonov–Bohm effect.

Acknowledgments

We are grateful for fruitful discussions with Fabrizio Nichele. We acknowledge financial support from the Swiss National Science Foundation and NCCR 'Quantum Science and Technology'.

References

[1] Topinka M A, LeRoy B J, Shaw S E J, Heller E J, Westervelt R M, Maranowski K D and Gossard A C 2000 *Science* **289** 2323
[2] Topinka M A, LeRoy B J, Westervelt R M, Shaw S E J, Fleischmann R, Heller E J, Maranowski K D and Gossard A C 2001 *Nature* **410** 183
[3] Paradiso N, Heun S, Roddaro S, Pfeifer L N, West K W, Sorba L, Biasiol G and Beltram F 2010 *Physica* E **42** 1038
[4] Kozikov A A, Rössler C, Ihn T, Ensslin K, Reichl C and Wegscheider W 2013 *New J. Phys.* **15** 013056
[5] Pioda A, Kicin S, Ihn T, Sigrist M, Fuhrer A, Ensslin K, Weichselbaum A, Ulloa S E, Reinwald M and Wegscheider W 2004 *Phys. Rev. Lett.* **93** 216801
[6] Fallahi P, Bleszynski A C, Westervelt R M, Huang J, Walls J D, Heller E J, Hanson M and Gossard A C 2005 *Nano Lett.* **5** 223
[7] Woodside M T and McEuen P L 2002 *Science* **296** 1098
[8] Hackens B *et al* 2006 *Nat. Physics* **2** 826
[9] Hackens B *et al* 2010 *Nat. Commun.* **1** 39
[10] Kozikov A A, Weinmann D, Rössler C, Ihn T, Ensslin K, Reichl C and Wegscheider W 2013 *New J. Phys.* **15** 083005
[11] Crook R, Smith C G, Graham A C, Farrer I, Beere H E and Ritchie D A 2003 *Phys. Rev. Lett* **91** 246803
[12] Aoki N, Brunner R, Burke A M, Akis R, Meisels R, Ferry D K and Ochiai Y 2012 *Phys. Rev. Lett* **108** 136804
[13] Ihn T 2004 *Electronic Quantum Transport in Mesoscopic Semiconductor Structures* (*Springer Tracts in Modern Physics* vol 192)
[14] Kouwenhoven L P, van Wees B J, Kool W, Harmans C J P M, Staring A A M and Foxon C T 1989 *Phys. Rev.* B **40** 8083